IPMU 11-0046
ICRR-Report-583-2010-16
CALT 68-2824

Direct Detection of Electroweak-Interacting Dark Matter

Junji Hisano[a,b], Koji Ishiwata[c], Natsumi Nagata[a,d], and Tomohiro Takesako[e]

[a] *Department of Physics, Nagoya University, Nagoya 464-8602, Japan*
[b] *Institute for the Physics and Mathematics of the Universe, University of Tokyo, Kashiwa 277-8568, Japan*
[c] *California Institute of Technology, Pasadena, CA 91125, USA*
[d] *Department of Physics, University of Tokyo, Tokyo 113-0033, Japan*
[e] *Institute for Cosmic Ray Research, University of Tokyo, Kashiwa 277-8582, Japan*

Abstract

Assuming that the lightest neutral component in an $SU(2)_L$ gauge multiplet is the main ingredient of dark matter in the universe, we calculate the elastic scattering cross section of the dark matter with nucleon, which is an important quantity for the direct detection experiments. When the dark matter is a real scalar or a Majorana fermion which has only electroweak gauge interactions, the scattering with quarks and gluon are induced through one- and two-loop quantum processes, respectively, and both of them give rise to comparable contributions to the elastic scattering cross section. We evaluate all of the contributions at the leading order and find that there is an accidental cancellation among them. As a result, the spin-independent cross section is found to be $\mathcal{O}(10^{-(46-48)})$ cm^2, which is far below the current experimental bounds.

1 Introduction

The existence of dark matter (DM) is one of the mysteries of the universe. Its energy density in the universe, which is about six times larger than that of baryon [1], cannot be explained in the standard model (SM) in particle physics. Weakly interacting massive particles (WIMPs) beyond the standard model are regarded as promising candidates for the DM. If they have TeV-scale masses, their relic abundance in the thermal history of universe may naturally account for the observed value. For the past years, a lot of efforts have been dedicated to the direct detection of WIMP DM, and their sensitivities have been improving. The XENON100 experiment [2], for example, has already started and announced its first result, which gives a stringent constraint on the spin-independent (SI) WIMP-nucleon elastic scattering cross section $\sigma_N^{\rm SI}$ ($\sigma_N^{\rm SI} < 2.4\times10^{-44}$ cm^2 for WIMPs with a mass 50 GeV [3]). Furthermore, ton-scale detectors for the direct detection experiments are now planned and expected to have significantly improved sensitivities.

Introduction of new particles with masses TeV scale is one of the simplest extensions of the SM in order to explain the DM in the universe if they are an electrically neutral component in an $SU(2)_L$ gauge multiplet (*n-tuplet*) with the hypercharge Y. We call them electroweak-interacting massive particles (EW-IMPs) in this article. EW-IMPs are assumed to interact with quarks and leptons only via weak gauge interactions. Neutral Wino and Higgsino in the minimal supersymmetric standard model (MSSM) are examples of such particles when the mixing with other states is negligible and squarks and sleptons are heavy enough. There is an earlier work [4] which studied the direct detection of Higgsino-like DM. They gave the cross section of Higgsino-like DM with nucleon by pointing out large loop contribution to Yukawa couplings. The cross sections of Wino/Higgsino DM with nucleon were calculated in Ref. [5]. In their study, they took into account electroweak loop corrections and showed that the SI interaction does not vanish in the large DM mass limit, which is a distinctive feature of EW-IMP DM. There are several other articles which give theoretical prediction for the cross section of EW-IMP DM. The authors in Ref. [6] intensively studied EW-IMP DM (they refer to it as Minimal dark matter), and a similar calculation was also performed in Ref. [7]. There is, however, inconsistency among Refs. [5, 6, 7]. In addition, interaction of gluon with EW-IMP, which is also one of the leading contributions in the EW-IMP DM-nucleon scattering, was neglected in the references. This point was first pointed out in Ref. [8].

In this paper, we give accurate prediction for EW-IMP-nucleon scattering in the direct detection experiments. Assuming that EW-IMPs are the main component of the DM in the universe, we calculate the cross section at the leading order of SM gauge couplings, including the gluon contribution. We provide the complete formulae for the EW-IMP DM-nucleon scattering cross section in a general form, and show that the SI cross section is below the current experimental bounds in all the cases we have studied. We also give numerical results for spin-dependent (SD) cross section.

This paper is organized as follows: in Section 2 we explain the EW-IMP DM scenario. In Section 3 general formulae of the elastic scattering cross section of dark matter with nucleon are summarized. In Section 4 we derive the cross section of the EW-IMP with

nucleon and show the numerical results. Section 5 is devoted to conclusion.

2 EW-IMP Dark Matter

As we described in the Introduction, EW-IMPs are an electrically neutral component in n-tuplet of $SU(2)_L$ with the hypercharge Y. In this section, we explain characteristics of EW-IMP DM assuming the EW-IMPs are fermionic. Fermionic EW-IMPs are popular, *e.g.*, Wino or Higgsino in the MSSM. We will discuss scalar EW-IMPs in the end of this section.

When the fermionic n-tuplet has only $SU(2)_L \times U(1)_Y$ gauge interactions in the SM and all the components have a common mass at tree level, the charged components become heavier than the neutral one because of quantum loop corrections [6]. The typical value of the mass difference ΔM is $\mathcal{O}(100)$ MeV. Thus, the neutral component of the multiplet could be a DM candidate in the universe if it is stable. It is found that fermionic EW-IMPs with $n \geq 5$ could be stable without imposing a certain symmetry to forbid its decay, such as R parity in the MSSM, since the gauge and Lorentz invariance prevent the DM candidate from decaying via the renormalizable interactions, and they turn out to be stable even if non-renormalizable effective operators are considered under the cut-off scale as large as the GUT-scale or Planck-scale [6, 9][1].

The thermal relic abundance could also explain the observed DM energy density when the EW-IMP mass is over 1 TeV for $n \geq 2$. In Ref. [10], the thermal relic abundance of Wino in the MSSM (which is EW-IMP with $n = 3$ and $Y = 0$) is evaluated.[2] The thermal relic abundances for EW-IMPs with $n = 2$ and 5 ($Y = 0$) are also evaluated [9]. According to those studies, the EW-IMP mass 1, 2.7, and 10 TeV is suggested in order to explain the observed DM abundance when $n = 2$, 3, and 5, respectively, and $Y = 0$.

Now we explicitly show the Lagrangian of EW-IMP DM scenario for our calculation. In the case of the multiplet with the hypercharge $Y = 0$, the following Lagrangian is introduced to the SM :

$$\Delta\mathcal{L} = \frac{1}{2}\overline{\tilde{\chi}}(i\not{D} - M_0)\tilde{\chi} \ , \tag{1}$$

where $\tilde{\chi}$ is an $SU(2)_L$ n-tuplet fermion, and $D_\mu = \partial_\mu - ig_1 Y B_\mu - ig_2 W^a_\mu T^a$ ($a = 1, 2, 3$) is the gauge covariant derivative. Here g_1 and g_2 is $U(1)_Y$ and $SU(2)_L$ gauge coupling constants, respectively, and T^a is for the generators of $SU(2)_L$ gauge group. The tree-level mass of the multiplet is denoted as M_0. The neutral component of the n-tuplet is a Majorana fermion, while the other charged components are Dirac fermions. The neutral component has no interaction with gauge bosons by itself so that the elastic scattering of EW-IMP with nucleon is induced via loop diagrams.

[1] In this article we implicitly suppose a symmetry to prevent EW-IMPs from decaying for $2 \leq n < 5$.

[2] In the evaluation of thermal relic abundance of EW-IMPs with $n > 2$, the Sommerfeld effect in the annihilation cross section of EW-IMP [11, 12] should be included [10].

On the other hand, for $Y \neq 0$ n-tuplet, the following term is added to the SM Lagrangian,

$$\Delta\mathcal{L} = \overline{\tilde{\psi}}(i\not{D} - M_0)\tilde{\psi} \ . \tag{2}$$

Here, $\tilde{\psi}$ is an $SU(2)_L$ n-tuplet Dirac fermion so that the fermion have an $SU(2)_L \times U(1)_Y$ invariant mass term. Note that Dirac fermions as the DM in the universe have been severely constrained by the direct detection experiments because of its large elastic scattering cross section via coherent vector interaction with target nuclei.

The situation changes if introducing the extra effective operators which give rise to a mass splitting δm between the left- and right-handed components of the neutral Dirac fermion after the electroweak symmetry breaking. In this case, the neutral component is no longer mass eigenstate; the mass splitting decomposes the neutral Dirac fermion, $\tilde{\psi}^0$, into two Majorana fermions, $\tilde{\chi}^0$ and $\tilde{\eta}^0$:

$$\tilde{\psi}^0 = \frac{1}{\sqrt{2}}(\tilde{\chi}^0 + i\tilde{\eta}^0). \tag{3}$$

Hereafter we treat $\tilde{\chi}^0$ as the lighter one, without loss of generality. Now the lighter component could be the DM candidate. It does not have any vector interaction by itself so that the DM-nucleon elastic scattering by Z-boson exchange is forbidden. In addition, if the mass splitting is large enough ($\delta m \gg \mathcal{O}(10)$ keV), the DM-nucleon *inelastic* scattering is suppressed kinematically. Thus, the EW-IMPs avoid the constraints from the direct detection experiments. On the other hand, large δm may also induce sizable contribution of the Higgs-boson exchange to the DM-nucleon scattering at tree level. To avoid all these constraints, in this article, we simply assume $\mathcal{O}(10)$ keV $\ll \delta m \ll \Delta M$ so that the elastic scattering of EW-IMP with nucleon is dominated by loop diagrams.

In the following discussion, we consider the scenarios with Majorana fermion EW-IMPs, with either $Y = 0$ or $Y \neq 0$. We simply express it as $\tilde{\chi}^0$ and the charged Dirac components which couple with $\tilde{\chi}^0$ as $\tilde{\psi}^{\pm}$.

It is straightforward to extend our calculation to scalar EW-IMPs. Contrary to the fermionic EW-IMPs, the scalar EW-IMPs have renormalizable self-interactions with Higgs boson, which contribute to the SI cross section of scalar EW-IMP with nucleon. When the interaction is suppressed enough to be ignored, elastic scattering of the EW-IMP with nucleon is induced by loop diagrams. In that case, the SI cross section of scalar EW-IMP with nucleon should agree with that of the fermionic EW-IMP when the EW-IMP mass is much larger than weak gauge boson masses. This is because the Lagrangians for both of fermionic and scalar EW-IMPs are the same in the non-relativistic limit or at the leading of the velocity expansion. Needless to say, the SD cross section of scalar EW-IMP with nucleon vanishes since the scalar EW-IMP has spin zero.

3 Effective Interactions for DM-Nucleon Scattering

In this section, we briefly review evaluation of the elastic scattering cross section of DM with nucleon, which is an important quantity for the direct detection experiments, as-

suming the DM is a Majorana fermion. The formulation given here is originally derived in Ref. [13]. See also Refs. [14, 15] for further details.

First, we write down the effective interactions of DM with light quarks ($q = u, d, s$) and gluon[3]:

$$\mathcal{L}^{\rm eff} = \sum_{q=u,d,s} \mathcal{L}_q^{\rm eff} + \mathcal{L}_g^{\rm eff} \ , \tag{4}$$

$$\begin{aligned}\mathcal{L}_q^{\rm eff} &= d_q\ \overline{\tilde{\chi}^0}\gamma^\mu\gamma_5\tilde{\chi}^0\ \bar{q}\gamma_\mu\gamma_5 q + f_q m_q\ \overline{\tilde{\chi}^0}\tilde{\chi}^0\ \bar{q}q \\ &+ \frac{g_q^{(1)}}{M}\ \overline{\tilde{\chi}^0} i\partial^\mu\gamma^\nu\tilde{\chi}^0\ \mathcal{O}^q_{\mu\nu} + \frac{g_q^{(2)}}{M^2}\ \overline{\tilde{\chi}^0}(i\partial^\mu)(i\partial^\nu)\tilde{\chi}^0\ \mathcal{O}^q_{\mu\nu} \ ,\end{aligned} \tag{5}$$

$$\mathcal{L}_g^{\rm eff} = f_G\ \overline{\tilde{\chi}^0}\tilde{\chi}^0 G^a_{\mu\nu}G^{a\mu\nu} \ . \tag{6}$$

Here, M and m_q are the masses of the DM and quarks, respectively. The field strength tensor of the gluon field is denoted by $G^a_{\mu\nu}$. The last two terms in Eq. (5) include the quark twist-2 operator, $\mathcal{O}^q_{\mu\nu}$, which is defined as,

$$\mathcal{O}^q_{\mu\nu} \equiv \frac{1}{2}\bar{q}i\left(D_\mu\gamma_\nu + D_\nu\gamma_\mu - \frac{1}{2}g_{\mu\nu}\not{D}\right)q \ . \tag{7}$$

The coefficients of the operators in Eqs. (5) and (6) are to be determined in the following section.

The cross section of DM with nucleon ($N = p, n$) is calculated from the effective Lagrangian in terms of SI and SD effective couplings, f_N and a_N,

$$\sigma_N = \frac{4}{\pi}m_R^2\left[|f_N|^2 + 3\,|a_N|^2\right] \ , \tag{8}$$

where $m_R \equiv Mm_N/(M+m_N)$ (m_N is nucleon mass). The SI and SD effective couplings are given as scattering matrix element of the effective Lagrangian between initial and final states. The results are

$$f_N/m_N = \sum_{q=u,d,s} f_q f_{Tq} + \sum_{q=u,d,s,c,b}\frac{3}{4}\left(q(2)+\bar{q}(2)\right)\left(g_q^{(1)}+g_q^{(2)}\right) - \frac{8\pi}{9\alpha_s}f_{TG}f_G \ , \tag{9}$$

$$a_N = \sum_{q=u,d,s} d_q\Delta q_N \ , \tag{10}$$

where

$$\langle N|m_q\bar{q}q|N\rangle/m_N = f_{Tq} \ , \ f_{TG} = 1 - \sum_{u,d,s} f_{Tq} \ , \tag{11}$$

$$\langle N(p)|\mathcal{O}^q_{\mu\nu}|N(p)\rangle = \frac{1}{m_N}(p_\mu p_\nu - \frac{1}{4}m_N^2 g_{\mu\nu})\ (q(2)+\bar{q}(2)) \ , \tag{12}$$

$$\langle N|\bar{q}\gamma_\mu\gamma_5 q|N\rangle = 2s_\mu\Delta q_N \ . \tag{13}$$

[3] We only keep the operators which give rise to the leading contributions for the DM-nucleon scattering with the non-relativistic velocity. Moreover, in order to remove the redundant terms, we use the integration by parts and the classical equation of motion for the operators when we construct the low-energy effective Lagrangian [16].

Mass fraction (for proton)	
f_{Tu}	0.023
f_{Td}	0.032
f_{Ts}	0.020
(for neutron)	
f_{Tu}	0.017
f_{Td}	0.041
f_{Ts}	0.020

Second moment at $\mu = m_Z$ (for proton)			
$u(2)$	0.22	$\bar{u}(2)$	0.034
$d(2)$	0.11	$\bar{d}(2)$	0.036
$s(2)$	0.026	$\bar{s}(2)$	0.026
$c(2)$	0.019	$\bar{c}(2)$	0.019
$b(2)$	0.012	$\bar{b}(2)$	0.012

Spin fraction (for proton)	
Δu_p	0.77
Δd_p	-0.49
Δs_p	-0.15

Table 1: Parameters for quark and gluon matrix elements used in this paper.

Here $\alpha_s \equiv g_s^2/4\pi$ (g_s is the coupling constant of $SU(3)_C$), $q(2)$ and $\bar{q}(2)$ are the second moments of the parton distribution functions (PDFs), and s_μ is the spin of the nucleon. Note the factor $1/\alpha_s$ in front of f_G in Eq. (9). It makes the gluon contribution comparable to the light-quark contribution, despite the interactions of DM with gluon are induced by higher-loop processes than those with light quarks [8]. In the present case, as discussed in the previous section, the DM-quark tree-level scattering is highly suppressed, and thus the one-loop processes become dominant for the DM-light quark effective interactions. Therefore, in order to give accurate prediction of the scattering cross section, we should evaluate not only the one-loop diagrams with light quarks but also the two-loop diagrams with gluon.

In Table 1 we list the numerical values for the parameters that we used in this article. The mass fractions of light quarks, f_{Tq} ($q = u, d, s$), are calculated using the results in Refs. [17, 18, 19]. The procedure for evaluating them is described in these references and Ref. [14]. The second moments of PDFs of quarks and anti-quarks are calculated at the scale $\mu = m_Z$ (m_Z is Z-boson mass) using the CTEQ parton distribution [20][4]. Finally, the spin fractions, Δq_N, in Eq. (13) are obtained from Ref. [22]. The second moments and the spin fractions for neutron are to be obtained by exchanging the values of up quark for those of down quark.

4 Results

4.1 Coefficients of the Effective Lagrangian

Now we evaluate the coefficients of the effective interactions displayed in Eqs. (5) and (6). From Eqs. (2) and (3), it is found that the EW-IMP, $\tilde{\chi}^0$, interacts with the weak gauge

[4]As will be described later, the terms with quark twist-2 operators in Eq. (5) are induced by the one-loop diagrams in which the loop momentum around the weak-boson mass scale yields dominant contribution. This fact verifies the use of the second moments of PDFs at the m_Z scale. See also discussion relevant to it in Ref. [21].

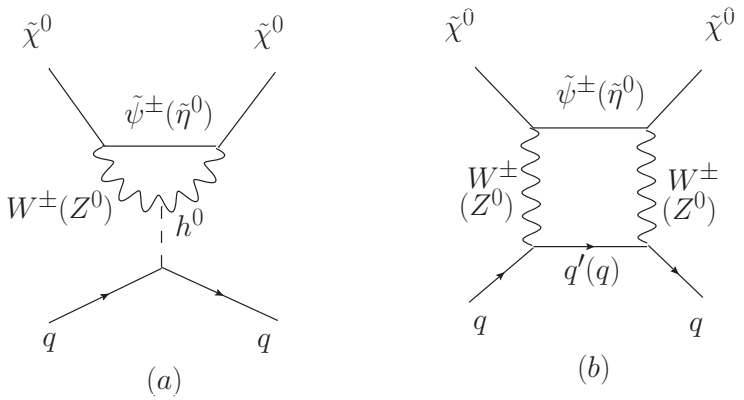

Figure 1: One-loop diagrams which induce effective interactions of EW-IMP DM with light quarks. There are also W-(Z-) boson crossing diagrams, which are not shown here.

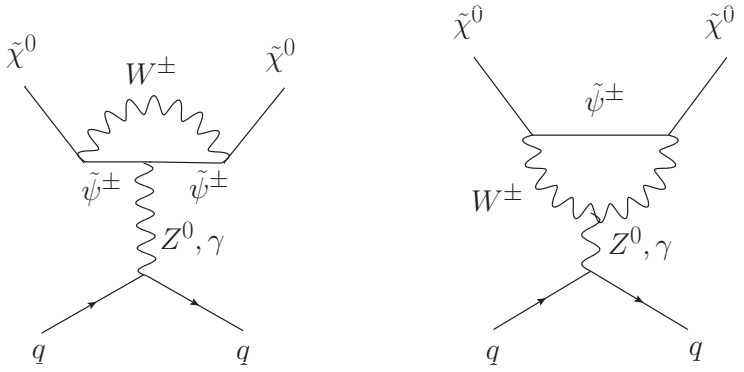

Figure 2: One-loop diagrams which correspond to the one-loop quantum correction to the EW-IMP-Z (γ) interaction vertex. These contributions turn out to vanish.

bosons ($W^{\pm}_{\mu}, Z^0_{\mu}$) as

$$\Delta\mathcal{L}_{\rm int.} = \left[\frac{g_2}{4}\sqrt{n^2-(2Y+1)^2}\;\overline{\tilde{\chi}^0}\gamma^{\mu}\tilde{\psi}^{-}\;W^{+}_{\mu} + \frac{g_2}{4}\sqrt{n^2-(2Y-1)^2}\;\overline{\tilde{\chi}^0}\gamma^{\mu}\tilde{\psi}^{+}\;W^{-}_{\mu} + \text{h.c.}\right] + \frac{ig_2(-Y)}{\cos\theta_W}\;\overline{\tilde{\chi}^0}\gamma^{\mu}\tilde{\eta}^0\;Z^0_{\mu}, \tag{14}$$

where θ_W is the weak mixing angle. The Majorana field $\tilde{\eta}^0$ is introduced for the cases of $Y \neq 0$. (See Eq. (3).) In either case ($Y = 0$ or $Y \neq 0$), the EW-IMP does not have any interaction by itself. Thus, it is loop diagrams that yield the leading contribution to the EW-IMP-nucleon elastic scattering cross section.

First, we consider the one-loop processes. The relevant diagrams are shown in Figs. 1 and 2. The diagrams in Fig. 1 give rise to the coefficients in Eq. (5) as

$$f_q = \frac{\alpha_2^2}{4m_h^2}\left[\frac{n^2-(4Y^2+1)}{8m_W}g_{\rm H}(w)+\frac{Y^2}{4m_Z\cos^4\theta_W}g_{\rm H}(z)\right]+\frac{\left((a_q^V)^2-(a_q^A)^2\right)Y^2}{\cos^4\theta_W}\frac{\alpha_2^2}{m_Z^3}g_{\rm S}(z), \tag{15}$$

$$d_q = \frac{n^2-(4Y^2+1)}{8}\frac{\alpha_2^2}{m_W^2}g_{\rm AV}(w)+\frac{2\left((a_q^V)^2+(a_q^A)^2\right)Y^2}{\cos^4\theta_W}\frac{\alpha_2^2}{m_Z^2}g_{\rm AV}(z), \tag{16}$$

$$g_q^{(1)} = \frac{n^2-(4Y^2+1)}{8}\frac{\alpha_2^2}{m_W^3}g_{\rm T1}(w)+\frac{2\left((a_q^V)^2+(a_q^A)^2\right)Y^2}{\cos^4\theta_W}\frac{\alpha_2^2}{m_Z^3}g_{\rm T1}(z), \tag{17}$$

$$g_q^{(2)} = \frac{n^2-(4Y^2+1)}{8}\frac{\alpha_2^2}{m_W^3}g_{\rm T2}(w)+\frac{2\left((a_q^V)^2+(a_q^A)^2\right)Y^2}{\cos^4\theta_W}\frac{\alpha_2^2}{m_Z^3}g_{\rm T2}(z). \tag{18}$$

Here, m_h and m_W are the masses of Higgs and W bosons, respectively, and $\alpha_2 = g_2^2/4\pi$. We also define the vector and axial-vector couplings of quarks with Z boson as

$$a_q^V = \frac{1}{2}T_{3q} - Q_q\sin^2\theta_W, \qquad a_q^A = -\frac{1}{2}T_{3q}, \tag{19}$$

where T_{3q} and Q_q denote the weak isospin and the charge of quark q, respectively. Furthermore, we parametrize $w \equiv m_W^2/M^2$ and $z \equiv m_Z^2/M^2$ in the above expressions. The first term in Eq. (15) is induced by the Higgs-boson exchange process, shown in diagram (a) of Fig. 1. The other terms in Eqs. (15-18) are all obtained from diagram (b). The mass functions, $g_H(x), g_S(x), g_{\rm AV}(x), g_{T1}(x)$, and $g_{T2}(x)$, in Eqs. (15-18) are given in Appendix A. We ignored the mass differences between $\tilde{\chi}^0$ and $\tilde{\psi}^\pm$ and also between $\tilde{\chi}^0$ and $\tilde{\eta}^0$ here. The loop integrals for the diagrams are finite, and they are dominated by the loop momentum around the weak-boson mass scale. We note here that some of these mass functions do not vanish in the limit of $w, z \to 0$ [5]. This implies that the SI interactions of EW-IMP with light quarks are not suppressed even if the EW-IMP mass is much larger than the gauge boson masses as we described in the Introduction. On the other hand, we found that both diagrams in Fig. 2 vanish separately by explicit calculation.

Next, let us move to the two-loop diagrams which yield the effective scalar coupling of EW-IMP with gluon, f_G. These diagrams are presented in Fig. 3. For each diagram, the gluon contributions are classified into two types in terms of the momentum scale which dominates in the loop integration. So-called "short-distance" contribution means that the momentum is typically masses of heavy particles, such as DM particle or the weak gauge bosons in the diagrams, and "long-distance" one means that the momentum is typically mass of quark in the loop diagrams. Among the latter one, the contributions in which the light quarks run are already incorporated in the mass fractions f_{T_q} defined in Eq. (11). Therefore, we do not need to add them in the calculation of the gluon contribution; otherwise we would doubly count them [14]. Consequently, the gluon contribution from each diagram is given by

$$f_G^{(i)} = \sum_{q=u,d,s,c,b,t} f_G^{(i)}|_q^{\rm SD} + \sum_{Q=c,b,t} c_Q f_G^{(i)}|_Q^{\rm LD}. \tag{20}$$

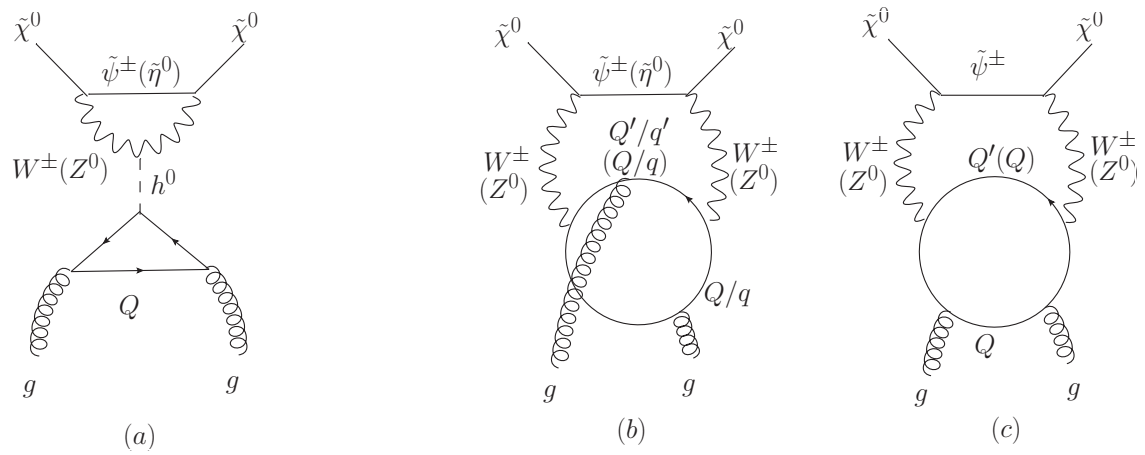

Figure 3: Relevant two-loop diagrams which contribute to effective scalar coupling of EW-IMP DM with gluon.There are also W-(Z-) boson crossing diagrams, which are not shown here.

Here $f_G^{(i)}|_q^{\rm SD}$ and $f_G^{(i)}|_q^{\rm LD}$ denote the short-distance and long-distance contributions of quark q in the loop in diagram (i) $(i = a, b, c)$ of Fig. 3, respectively. We also take into account large QCD corrections in the long-distance contributions [23] by using $c_Q = 1+11\alpha_s(m_Q)/4\pi$ $(Q = c, b, t)$. We take $c_c = 1.32, c_b = 1.19$, and $c_t = 1$ for $\alpha_s(m_Z) = 0.118$ in our calculation. Note that the long-distance contribution is gauge invariant. This is because its contribution to the operator $f_G G^a_{\mu\nu} G^{a\mu\nu}$ is evaluated from scalar-type effective operator $f_q m_q \bar{q} q$ [13, 14]. (See also later discussion where the explicit calculations are given.) Consequently, the gauge invariance of the short-distance contribution is guaranteed since summation of the both contribution is obviously gauge invariant. Then, the effective coupling of EW-IMP with gluon is obtained as

$$f_G = f_G^{(a)} + f_G^{(b)} + f_G^{(c)} \ . \tag{21}$$

Let us see each diagram closely. It is obvious that diagram (a) gives the long-distance contribution. Thus, we sum up for heavy quarks in the loop, and get

$$f_G^{(a)} = -\frac{\alpha_s}{12\pi} \times \frac{\alpha_2^2}{4m_h^2} \sum_{Q=c,b,t} c_Q \left[\frac{n^2 - (4Y^2+1)}{8m_W} g_{\rm H}(w) + \frac{Y^2}{4m_Z \cos^4\theta_W} g_{\rm H}(z) \right] \ . \tag{22}$$

Here the first and second terms in the bracket come from W- and Z-boson exchanges, respectively. As we described above, this long-distance contribution is given by effective scalar-type coupling (of the Higgs contribution) as $-\frac{\alpha_s}{12\pi} f_Q$.

For the calculation of diagrams (b) and (c), on the other hand, we follow the steps supplied in Ref. [14]. In the work, the systematic calculation for the W-boson exchange diagrams at two-loop level in the Wino DM scenario is given. The procedure is applicable to compute the two-loop diagrams in our case. For the W-boson exchange diagrams, the

analytic result is simply given by multiplying a factor $(n^2-(4Y^2+1))/8$ to their result of the Wino DM case. (as the first term in Eq. (22)). Even for the Z-boson exchange contribution, the calculation is straightforward extension. In the following we outline the calculation and give the result of the Z-boson exchange contribution.

First, we calculate the vacuum polarization tensor of Z boson in the gluon background field, $\Pi^Z_{\mu\nu}(p)$. It is given as

$$\begin{aligned} &i\Pi^Z_{\mu\nu}(p) \\ &= -\sum_{[q]}\int \frac{\mathrm{d}^4 l}{(2\pi)^4}\frac{g_2^2}{\cos^2\theta_W}\ \mathrm{Tr}_{\mathrm{L+C}}\{\gamma_\mu(a_q^V+a_q^A\gamma_5)S_q(l)\gamma_\nu(a_q^V+a_q^A\gamma_5)\tilde{S}_q(l-p)\}, \end{aligned} \tag{23}$$

where $\mathrm{Tr}_{\mathrm{L+C}}$ denotes the trace over the Lorentz and color indices, and $[q]$ means the sum is taken over all quarks for the short-distance contribution and heavy quarks for the long-distance contribution. The quark propagators $S_q(p)$ and $\tilde{S}_q(p)$ are under the gluon background field with the Fock-Schwinger gauge. (See Appendix A in Ref. [14].) We decompose the polarization function as

$$\Pi^Z_{\mu\nu}(p) = \left(-g_{\mu\nu}+\frac{p_\mu p_\nu}{p^2}\right)\ \Pi^Z_T(p^2)+\frac{p_\mu p_\nu}{p^2}\ \Pi^Z_L(p^2). \tag{24}$$

By the explicit calculation, we found that the longitudinal part $\Pi_L(p^2)$ does not contribute to f_G[5]. Thus, we only calculate transverse component, $\Pi^Z_T(p^2)$. The contributions from diagrams (b) and (c) to $\Pi^Z_T(p^2)$ are given as

$$\begin{aligned} \left[\Pi^Z_T(p^2)\right]^q_{(b)}|_{GG} &= \frac{\alpha_2\alpha_s}{6\cos^2\theta_W}(G^a_{\mu\nu})^2\left[(a_q^V)^2+(a_q^A)^2\right]\left[p^2(B_1^{(2,2)}+B_{21}^{(2,2)})+6B_{22}^{(2,2)}\right], \\ \left[\Pi^Z_T(p^2)\right]^q_{(c)}|_{GG} &= \frac{2\alpha_2\alpha_s}{\cos^2\theta_W}(G^a_{\mu\nu})^2 m_q^2\big[\{(a_q^V)^2+(a_q^A)^2\}(-p^2B_1^{(4,1)}+2B_{22}^{(4,1)}) \\ &\qquad -2(a_q^A)^2(p^2B_{21}^{(4,1)}+4B_{22}^{(4,1)})\big], \end{aligned} \tag{25}$$

where $\left[\Pi^Z_T(p^2)\right]^q_{(i)}$ denotes the contribution from diagram (i) $(i=b,c)$ with quark q running in the loop. Here, "$|_{GG}$" represents that we keep only the terms which are proportional to $G^a_{\mu\nu}G^{a\mu\nu}$ in the polarization function, since the terms proportional to $G^a_{\mu\nu}G^{a\mu\nu}$ contribute to f_G. The loop functions in Eq. (25) are defined as follows:

$$p^\mu B_1^{(n,m)} \equiv \int\frac{d^4k}{i\pi^2}\frac{k^\mu}{[k^2-m_q^2]^n[(k+p)^2-m_q^2]^m}\ , \tag{26}$$

$$p^\mu p^\nu B_{21}^{(n,m)}+g^{\mu\nu}B_{22}^{(n,m)} \equiv \int\frac{d^4k}{i\pi^2}\frac{k^\mu k^\nu}{[k^2-m_q^2]^n[(k+p)^2-m_q^2]^m}\ . \tag{27}$$

[5] This is consistent with the fact that EW-IMPs have no tree-level coupling with Higgs boson and Goldstone bosons of the electroweak symmetry breaking, which turn into the longitudinal modes of Z and W bosons.

As is the same in the calculation of two-loop W-boson exchange diagrams discussed in Ref. [14], the diagrams (b) and (c) yield the short-distance contribution and long-distance contribution, respectively. We have checked this identification by explicit calculation. This is also confirmed from the fact that the long distance-contribution corresponds to the one which is calculated from quark triangle diagram using effective scalar-type coupling f_q in the M and $m_{W/Z} \to \infty$ limit [14], as we mentioned before. Therefore, $\Pi_T^Z(p^2)|_{GG}$ is obtained as

$$\Pi_T^Z(p^2)|_{GG} = \sum_{q=u,d,s,c,b,t} \left[\Pi_T^Z(p^2)\right]_{(b)}^q |_{GG} + \sum_{Q=c,b,t} c_Q \left[\Pi_T^Z(p^2)\right]_{(c)}^Q |_{GG}. \tag{28}$$

The results of $\left[\Pi_T^Z(p^2)\right]_{(b)}^q |_{GG}$ and $\left[\Pi_T^Z(p^2)\right]_{(c)}^Q |_{GG}$ are given in Appendix B.

With these Z-boson polarization functions, we get the contribution from Z-boson exchange diagrams at two-loop level. Combining it with the contribution from W-boson exchange diagrams, we eventually obtain the effective coupling f_G from diagrams (b) and (c) as

$$f_G^{(b)} + f_G^{(c)} = \frac{\alpha_s \alpha_2^2}{4\pi} \left[\frac{n^2 - (4Y^2+1)}{8 m_W^3} g_{\rm W}(w,y) + \frac{Y^2}{4 m_Z^3 \cos^4\theta_W} g_{\rm Z}(z,y) \right] , \tag{29}$$

where $y \equiv m_t^2/M^2$ (m_t is the top quark mass), and the mass functions, $g_{\rm W}(z,y)$ and $g_{\rm Z}(z,y)$, are given in Appendix B. We ignore the mass of quarks except that of top quark in this computation.

4.2 Spin-independent and Spin-dependent Cross Sections

With the effective couplings derived above, we evaluate the cross section of EW-IMP with nucleon. First, we discuss the SI cross section. In order to look over the behavior of the cross section, we plot the SI cross section as a function of the EW-IMP mass in Fig. 4. In this figure, we set $n = 5$ and $Y = 2$ as an example of the case where both W- and Z-boson exchange diagrams contribute, and take Higgs-boson mass as m_h =130, 115, 300 and 500 GeV from bottom to top. It is found that the SI cross section has little dependence on the EW-IMP mass when the mass is larger than $\mathcal{O}(1)$ TeV. We have checked such a behavior for other n and Y cases. The cross section ranges from 10^{-47} cm^2 to 10^{-46} cm^2 in this figure when Higgs-boson mass increased from $m_h = 115$ GeV to 500 GeV. (Although it is not monotonic.)

In Fig. 5, we plot the EW-IMP-proton SI cross section as a function of Higgs-boson mass for $n = 5$ (left panel) and both $n = 2$ and $n = 3$ (right panel). The EW-IMP mass is taken to be equal to 1, 2.7, and 10 TeV for $n = 2$, 3, and 5, respectively[6] [9, 10]. It is seen that the cross section is enhanced as n is larger and Y is smaller. This behavior will

[6] Recall that the EW-IMP mass $M = 1,\ 2.7$, and 10 TeV is suggested in order to explain the observed DM abundance when $n = 2,\ 3$, and 5, respectively, and $Y = 0$. The thermal relic abundance of the EW-IMP has not been evaluated when $Y \neq 0$. We use those suggested values in $Y \neq 0$ case since the SI cross section is insensitive to the EW-IMP mass as mentioned in the text.

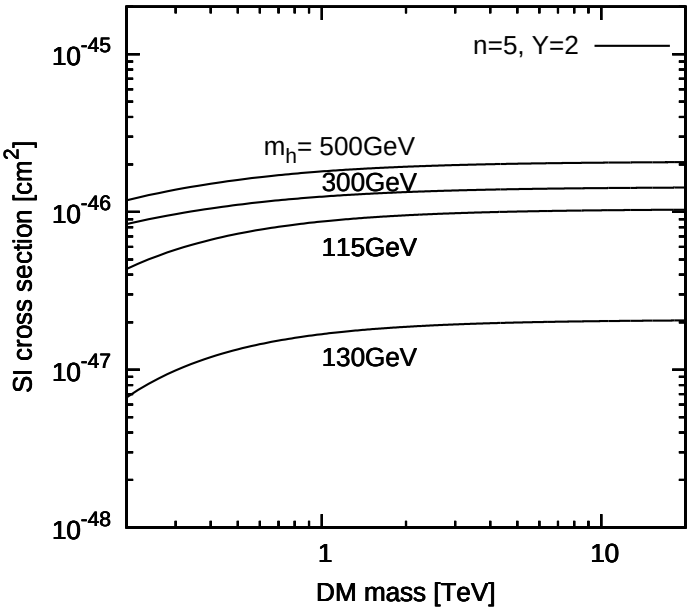

Figure 4: DM-proton SI cross section for $n = 5$ and $Y = 2$. We take Higgs-boson mass as m_h =130, 115, 300 and 500 GeV from bottom to top in this figure.

be explained later. We also found that the SI cross section of EW-IMP with nucleon is far below the current experimental bound. This is the consequence of the calculation in which all the relevant terms at leading order are taken into account. The suppression of the cross section originates in an accidental cancellation within the SI effective coupling, f_N. Such an cancellation was already pointed out for the Wino dark matter, *i.e.* $n = 3$ with $Y = 0$ [8]. In our calculation, we found that the similar cancellation also occurs in general n-tuplet cases with both W-boson and Z-boson contributions.

Let us examine what happens in the SI effective coupling. In Fig. 6, we show the contribution to f_p/m_p of each effective coupling in Eq. (9). The left (right) panel in the figure shows each contribution due to the W-boson (Z-boson) loops as a function of Higgs-boson mass. The plot is given in units of $(n^2 - (4Y^2 + 1))/8$ and Y^2 in left and right panels, respectively. In the figure, we show the contribution of the Higgs-boson exchange including both one- and two-loop contributions (solid), the gluon contribution except for the Higgs-boson contribution (dashed), the quark twist-2 operator contribution (dash-dotted), and the contribution to the quark scalar-type operators with the coefficient f_q from the Z-boson box diagrams (double-dashed). The W-boson box diagrams do not generate the scalar-type operators [8]. It is found that the contributions from the twist-2 operators generated by both W-boson and Z-boson loops are positive, while all the other contributions are negative. In addition, they have roughly the same order in absolute value. This is why the cancellation happens in the SI effective coupling induced by each W-boson and Z-boson contribution. We also find that the Z-boson contribution in

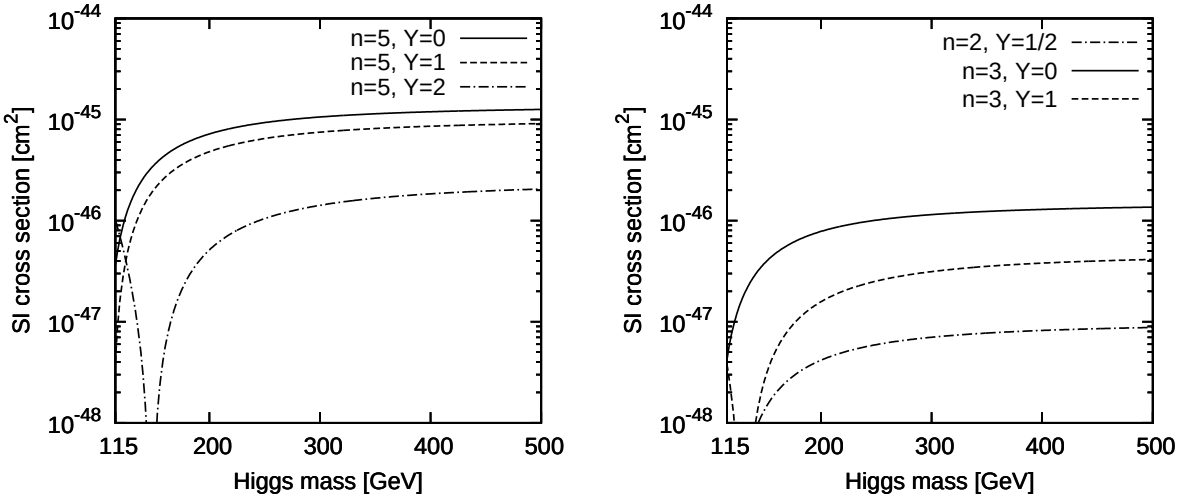

Figure 5: SI cross sections of DM-proton elastic scattering as a function of Higgs-boson mass for $n = 5$ (left panel) and $n = 2, 3$ (right panel). We take $M = 1$, 2.7, 10 TeV for n =2, 3, and 5, respectively. In left panel, solid, dashed, and dash-dotted lines represent $n = 5$ with $Y = 0$, 1, and 2 cases, respectively. In right panel $(n, Y) = (3, 0)$, $(3, 1)$, and $(2, 1/2)$ correspond to solid, dashed, and dash-dotted lines, respectively.

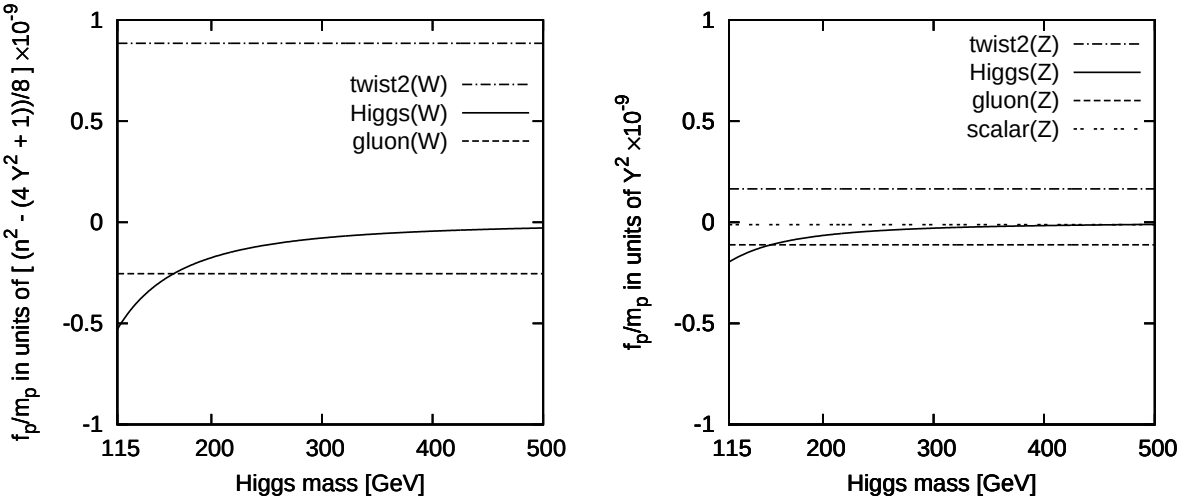

Figure 6: The contributions of each effective coupling in Eq. (9) to f_p/m_p. Left panel shows each contribution from W-boson loops as a function of Higgs-boson mass, while right one illustrates contribution by Z-boson loops. These plots are shown in units of $(n^2 - (4Y^2 + 1))/8$ and Y^2, respectively. We take $M = 10$ TeV. In the both panels, solid line represents the contribution of the Higgs-boson exchange (including both one- and two-loop contribution), dashed line indicates the rest of gluon contribution in the two-loop contribution, and dash-dotted line denotes that from quark twist-2 operators. Double-dashed line in right graph shows contribution of scalar-type operator coming from box diagrams.

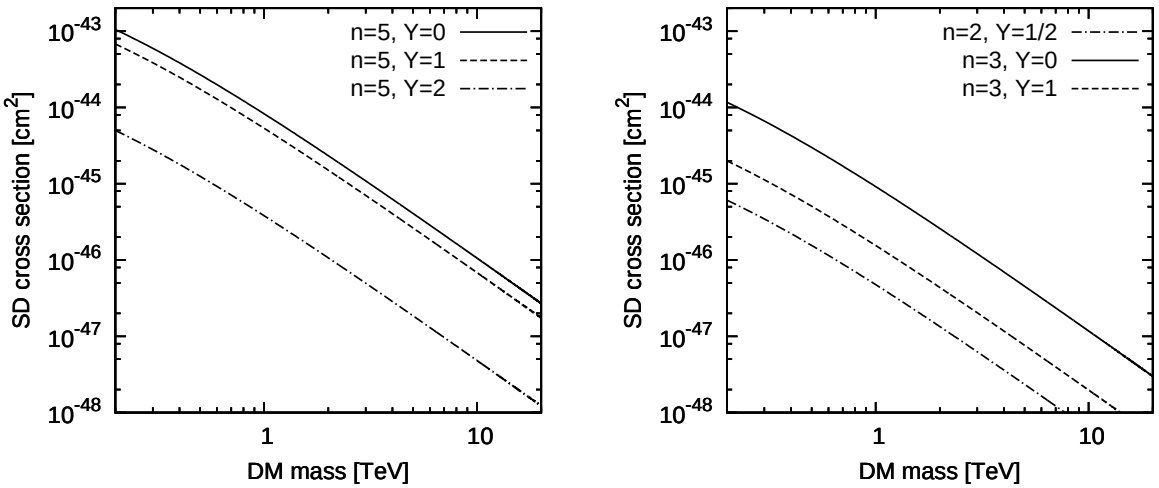

Figure 7: SD cross section of DM-proton elastic scattering for $n = 5$ (left) and $n = 2, 3$ (right). In left graph, solid line, dashed line, and dash-dotted line represent $Y = 0$, 1, 2, while in right graph they represents $(n, Y) = (3, 0)$, (3,1), (2, 1/2), respectively.

units of Y^2 is generally rather small compared with the W-boson contribution in units of $(n^2 - (4Y^2 + 1))/8$. Consequently, the cross section is suppressed when Y gets larger (because the coupling between W boson and EW-IMP is suppressed). When Higgs-boson mass is relatively small as $m_h \sim 115 - 200$ GeV, the contribution of Higgs-boson exchange becomes large. Then, there is much more significant cancellation within each W- and Z-boson contribution. As a result, these cancellations give rise to a very suppressed SI cross section.

Next, we show the SD cross section in Fig. 7 for completeness. Since the SD cross section is independent of Higgs-boson mass, we plot it as a function of the EW-IMP mass. Contrary to the SI cross section, the SD cross section is suppressed when the EW-IMP mass is larger [5]. In the left panel, the SD cross sections of $n = 5$ cases with $Y = 0,\ 1,$ and 2 are shown in the solid line, the dashed line, and the dash-dotted line, respectively. In the right panel, we give the cross sections by taking $(n, Y) = (3, 0)$, (3,1) and (2, 1/2), in the solid line, the dashed line, and the dash-dotted line, respectively. [7] As expected, the cross section is enhanced by larger n in a similar way to the SI cross section. The figure also shows that the cross section decreases when one sets Y larger, because the contribution from W-boson exchange reduces. We also find that the contribution from Z-boson exchange has the opposite sign and rather small significance compared to that from W-boson loop diagrams.

Throughout the calculation, we have ignored the mass splitting δm between the neutral components for $Y \neq 0$ case. The magnitude of δm is model-dependent. If δm is relatively large against our assumption, the Higgs-boson exchange contribution at tree level becomes significant, and one might expect a larger SI cross section. Even in such a case, the

[7] There was an numerical error in the result of SD cross section in Ref. [8]. We have corrected it here.

extension is straightforward.

Lastly, we refer to the difference between our results and previous works. It is found that the mass functions in Eq. (30) in the Appendix A which gives scalar- and twist-2-type (and also axial-type) contributions agree with the corresponding loop functions given in Eq. (42) of Ref. [5], except for $F_{S2}^{(0)}(x)$ and $F_{T1}^{(0)}(x)$ in Ref. [5]. (This was previously described in Ref. [8].) On the other hand, gluon contribution was taken into account without explicit calculation; however, the sign of the contribution is the same with our result. As a consequence, similarly to our result, the cancellations between each contribution happen and the cross sections computed in their works are comparable to our results.

On the other hand, the SI cross sections in Refs. [6, 7] are larger than our results by more than an order of magnitude. In Ref. [6] only the scalar-type operator is taken into account in the limit $M \gg m_W \gg m_q$, which does not agree with our result in the same limit. Although they mention the twist-2 type contribution, they took into account this contribution in the same sign as the scalar-type one. Moreover, the gluon contribution is omitted. Thus, there is no cancellation which we found in the effective coupling, to give rise to the large cross section.

In Ref. [7], the explicit results of the loop calculation are given. However, all of the loop functions except $f_I^Z(x)$ in Eq. (26) in Ref. [7] are different from ours. To check their result further, we compare them with ours in the limit $m_{W/Z}/M \to 0$. In Eq. (15), which is scalar-type contribution, the first term (of the first parenthesis) agree with their result except for the sign, and the other terms are $-1/2$ of corresponding term in their work. For twist-2 type contributions, the one (*i.e.*, Eq. (17)) is the same as their result in the limit, while another contribution (*i.e.*, Eq. (18)) is neglected in their paper. The gluon contribution is considered, but not evaluated properly. As a result, the cancellation we found in our calculation does not occur, which makes the resultant cross section large.

5 Conclusion

We have studied the direct detection of EW-IMP DM, which is the lightest neutral component of an $SU(2)_L$ multiplet interacting with quarks and leptons only through the $SU(2)_L \times U(1)_Y$ gauge interactions. Although EW-IMP DM does not scatter off nucleon at tree level, it does at loop level, and the SI scattering cross section is not suppressed even if the mass of EW-IMP is much larger than gauge boson mass. We evaluate the two-loop processes for the EW-IMP-gluon interaction in addition to the one-loop processes of EW-IMP scattering with light quarks, since both of them yield considerable contribution to the SI scattering cross section. As a result, the SI cross section is found to be $\mathcal{O}(10^{-(46-48)})$ cm^2, depending on Higgs-boson mass, the number of components n in the multiplet, and the hypercharge Y of the EW-IMP DM. Such small value of the cross section is due to an accidental cancellation in the SI effective coupling. This cancellation is a general feature for EW-IMP DM, and thus makes it difficult to catch EW-IMP DM in the direct detection experiments in the near future.

Acknowledgments

This work is supported by Grant-in-Aid for Scientific research from the Ministry of Education, Science, Sports, and Culture (MEXT), Japan, No. 20244037, No. 20540252, and No. 22244021 (J.H.), and also by World Premier International Research Center Initiative (WPI Initiative), MEXT, Japan. This work was also supported in part by the U.S. Department of Energy under contract No. DE-FG02-92ER40701, and by the Gordon and Betty Moore Foundation (K.I.).

Appendix

In this Appendix we provide the mass functions and the Z-boson vacuum polarization functions, both presented in Section 4.

A Mass Functions from One-loop Diagrams

The mass functions used in Eqs. (15-18) in the calculation of one-loop diagrams are

$$\begin{aligned}
g_{\rm H}(x) &= -\frac{2}{b_x}(2+2x-x^2)\tan^{-1}\left(\frac{2b_x}{\sqrt{x}}\right)+2\sqrt{x}(2-x\log(x))\ , \\
g_{\rm S}(x) &= \frac{1}{4b_x}(4-2x+x^2)\tan^{-1}\left(\frac{2b_x}{\sqrt{x}}\right)+\frac{1}{4}\sqrt{x}(2-x\log(x))\ , \\
g_{\rm AV}(x) &= \frac{1}{24b_x}\sqrt{x}(8-x-x^2)\tan^{-1}\left(\frac{2b_x}{\sqrt{x}}\right)-\frac{1}{24}x(2-(3+x)\log(x))\ , \\
g_{\rm T1}(x) &= \frac{1}{3}b_x(2+x^2)\tan^{-1}\left(\frac{2b_x}{\sqrt{x}}\right)+\frac{1}{12}\sqrt{x}(1-2x-x(2-x)\log(x))\ , \\
g_{\rm T2}(x) &= \frac{1}{4b_x}x(2-4x+x^2)\tan^{-1}\left(\frac{2b_x}{\sqrt{x}}\right)-\frac{1}{4}\sqrt{x}(1-2x-x(2-x)\log(x))\ , \qquad (30)
\end{aligned}$$

with $b_x \equiv \sqrt{1-x/4}$.

B Mass functions from Two-loop Diagrams

Here, we present the polarization functions and the mass functions for Z boson. Performing the integration in Eq.(25), we derive the polarization functions as

$$\begin{aligned}
\left[\Pi_T^Z(p^2)\right]^q_{(b)}|_{GG} &= \frac{\alpha_2\alpha_s}{6\cos^2\theta_W}(G^a_{\mu\nu})^2\left[(a_q^V)^2+(a_q^A)^2\right] \\
&\times\frac{2(p^2-4m_q^2)(p^2-3m_q^2)+4m_q^2(p^2-6m_q^2)\sqrt{\frac{4m_q^2}{p^2}-1}\cot^{-1}\left(\sqrt{\frac{4m_q^2}{p^2}-1}\right)}{p^2(p^2-4m_q^2)^2}\ ,
\end{aligned}$$

$$\left[\Pi_T^Z(p^2)\right]^q_{(c)}|_{GG} = -\frac{\alpha_2\alpha_s}{3\cos^2\theta_W}(G^a_{\mu\nu})^2\Bigg[\frac{(a_q^V)^2\left(2p^4-11m_q^2p^2+24m_q^4\right)-(a_q^A)^2(p^2-4m_q^2)(2p^2-3m_q^2)}{p^2(p^2-4m_q^2)^2}+$$
$$\frac{2m_q^2\sqrt{\frac{4m_q^2}{p^2}-1}\left\{\left(p^4-22m_q^2p^2+48m_q^4\right)(a_q^V)^2+(a_q^A)^2(p^2-4m_q^2)(p^2+6m_q^2)\right\}\cot^{-1}\left(\sqrt{\frac{4m_q^2}{p^2}-1}\right)}{p^2(p^2-4m_q^2)^3}\Bigg], \tag{31}$$

and in the limit of zero quark mass, these functions lead to

$$\begin{aligned}\left[\Pi_T^Z(p^2)\right]^q_{(b)}|_{GG} &\to \frac{\alpha_2\alpha_s}{3\cos^2\theta_W}(G^a_{\mu\nu})^2\left[(a_q^V)^2+(a_q^A)^2\right]\frac{1}{p^2}\,,\\ \left[\Pi_T^Z(p^2)\right]^q_{(c)}|_{GG} &\to -\frac{2\alpha_2\alpha_s}{3\cos^2\theta_W}(G^a_{\mu\nu})^2\left[(a_q^V)^2-(a_q^A)^2\right]\frac{1}{p^2}\,.\end{aligned} \tag{32}$$

Using the polarization functions, we compute $g_{\rm Z}(z,y)$ in Eq.(29) as

$$g_{\rm Z}(z,y) = \left[\sum_{q=u,d,s,c,b}\left\{(a_q^V)^2+(a_q^A)^2\right\}-2\sum_{Q=c,b}c_Q\left\{(a_q^V)^2-(a_q^A)^2\right\}\right]\times 4g_{\rm B1}(z)+g_t(z,y)\,. \tag{33}$$

Here, the first term comes from the contribution of all quarks except top quark, and c_Q in it represents the QCD corrections in the long-distance contributions [23]. The second term $g_t(z,y)$ is the contribution of top quark. The function $g_{\rm B1}(x)$ is given as

$$g_{\rm B1}(x) = -\frac{1}{24}\sqrt{x}(x\log(x)-2)+\frac{(x^2-2x+4)\tan^{-1}(\frac{2b_x}{\sqrt{x}})}{24b_x}\,, \tag{34}$$

which is equal to the one in Ref. [8]. In the calculation of $g_t(z,y)$, we decompose it into two parts:

$$g_t(z,y) = g_t^{\text{no-log}}(z,y)+g_t^{\log}(z,y). \tag{35}$$

$g_t^{\text{no-log}}(z,y)$ is analytically obtained as

$$g_t^{\text{no-log}}(z,y) = (a_t^V)^2\ G_{t1}(z,y)+(a_t^A)^2\ G_{t2}(z,y), \tag{36}$$

where

$$\begin{aligned}G_{t1}(z,y) = &-\frac{\sqrt{z}(12y^2-zy+z^2)}{3(4y-z)^2}\\ &+\frac{z^{3/2}(48y^3-20zy^2+12z^2y-z^3)}{6(4y-z)^3}\ \log z+\frac{2z^{3/2}y^2(4y-7z)}{3(4y-z)^3}\ \log(4y)\\ &-\frac{z^{3/2}\sqrt{y}(16y^3-4(2+7z)y^2+14(2+z)y+5z)}{3(4y-z)^3\sqrt{1-y}}\ \tan^{-1}\left(\frac{\sqrt{1-y}}{\sqrt{y}}\right)\\ &-\tan^{-1}\left(\frac{\sqrt{4-z}}{\sqrt{z}}\right)\\ &\times\frac{48(z^2-2z+4)y^3-4z(5z^2-10z+44)y^2+12z^3(z-2)y-z^3(z^2-2z+4)}{3(4y-z)^3\sqrt{4-z}},\end{aligned}$$

$$
\begin{aligned}
G_{t2}(z,y) = {} & \frac{\sqrt{z}(2y-z)}{(4y-z)} - \frac{z^{3/2}(8y^2-8zy+z^2)}{2(4y-z)^2}\ \log z - \frac{4z^{3/2}y^2}{(4y-z)^2}\ \log(4y) \\
& + \frac{4z^{3/2}\sqrt{y}(2y^2-y-1)}{(4y-z)^2\sqrt{1-y}}\ \tan^{-1}\left(\frac{\sqrt{1-y}}{\sqrt{y}}\right) \\
& - \frac{8z(z^2-2z+1)y-(z^2-2z+4)(8y^2+z^2)}{(4y-z)^2\sqrt{4-z}}\ \tan^{-1}\left(\frac{\sqrt{4-z}}{\sqrt{z}}\right).
\end{aligned}
\tag{37}
$$

On the other hand, we calculate $g_t^{\log}(z,y)$ numerically. For convenience, we rewrite it as

$$
g_t^{\log}(z,y) = 4z^{3/2}y^2\left(A_1\ y\ [I_1+I_2] + A_2\ [I_3+I_4]\right), \tag{38}
$$

with

$$
\begin{aligned}
A_1 &= -2(a_t^V)^2 + 4(a_t^A)^2, \\
A_2 &= -(a_t^V)^2 + (a_t^A)^2,
\end{aligned}
\tag{39}
$$

and then carry out the following integrals numerically,

$$
\begin{aligned}
I_1 &= \int_0^\infty \mathrm{d}t\ \frac{(\sqrt{t+4}-\sqrt{t})\left(\log\left[\sqrt{t+4y}+\sqrt{t}\right]-\log\left[\sqrt{t+4y}-\sqrt{t}\right]\right)}{[t+z]^2\ [t+4y]^{5/2}\ t}, \\
I_2 &= \int_0^\infty \mathrm{d}t\ \frac{1}{2}\times\frac{(t+2-\sqrt{t}\sqrt{t+4})\left(\log\left[\sqrt{t+4y}+\sqrt{t}\right]-\log\left[\sqrt{t+4y}-\sqrt{t}\right]\right)}{[t+z]^2\ [t+4y]^{5/2}\ t^{1/2}}, \\
I_3 &= \int_0^\infty \mathrm{d}t\ \frac{(\sqrt{t+4}-\sqrt{t})\left(\log\left[\sqrt{t+4y}+\sqrt{t}\right]-\log\left[\sqrt{t+4y}-\sqrt{t}\right]\right)}{[t+z]^2\ [t+4y]^{5/2}}, \\
I_4 &= \int_0^\infty \mathrm{d}t\ \frac{1}{2}\times\frac{\sqrt{t}(t+2-\sqrt{t}\sqrt{t+4})\left(\log\left[\sqrt{t+4y}+\sqrt{t}\right]-\log\left[\sqrt{t+4y}-\sqrt{t}\right]\right)}{[t+z]^2\ [t+4y]^{5/2}}.
\end{aligned}
$$

Lastly, we present the mass function $g_{\rm W}(w,y)$ in Eq. (29), which is readily obtained by following the similar procedure described in Ref. [8]:

$$
g_{\rm W}(w,y) = 2g_{\rm B1}(w) + g_{\rm B3}(w,y) \tag{40}
$$

with

$$
g_{\rm B3}(x,y) = g_{\rm B3}^{(1)}(x,y) + c_b g_{\rm B3}^{(2)}(x,y). \tag{41}
$$

Here the first term of $g_{\rm W}(w,y)$ is coming from the first- and second-generation quark loop diagrams, while the second term is from the third-generation quark loop diagrams. The mass function $g_{\rm B1}(x)$ is displayed in Eq. (34). Although we use the same symbol for $g_{\rm B3}(x,y)$ as in Ref. [8], it is reevaluated with the QCD correction for the long-distance contributions, which we illustrate with the factor c_b in Eq. (41) explicitly. We have checked numerically that including the QCD correction changes the SI cross section by up to a

few %. The functions $g^{(1)}_{\rm B3}(x,y)$ and $g^{(2)}_{\rm B3}(x,y)$ are analytically given as

$$
\begin{aligned}
g^{(1)}_{\rm B3}(x,y) &= \frac{-x^{3/2}}{12(y-x)} + \frac{-x^{3/2}y^2}{24(y-x)^2}\log y - \frac{x^{5/2}(x-2y)}{24(y-x)^2}\log x \\
&\quad - \frac{x^{3/2}\sqrt{y}(y+2)\sqrt{4-y}}{12(y-x)^2}\,\tan^{-1}\left(\frac{\sqrt{4-y}}{\sqrt{y}}\right) \\
&\quad + \frac{x(x^3-2(y+1)x^2+4(y+1)x+4y)}{12(y-x)^2\,\sqrt{4-x}}\,\tan^{-1}\left(\frac{\sqrt{4-x}}{\sqrt{x}}\right), \\
g^{(2)}_{\rm B3}(x,y) &= \frac{-x^{3/2}y}{12(y-x)^2} + \frac{-x^{5/2}y^2}{24(y-x)^3}\log y + \frac{x^{5/2}y^2}{24(y-x)^3}\log x \\
&\quad + \frac{x^{3/2}\sqrt{y}(-6y+xy^2-2xy-2x)}{12(y-x)^3\,\sqrt{4-y}}\,\tan^{-1}\left(\frac{\sqrt{4-y}}{\sqrt{y}}\right) \\
&\quad + \frac{-xy(x^2y-2xy-6x-2y)}{12(y-x)^3\,\sqrt{4-x}}\,\tan^{-1}\left(\frac{\sqrt{4-x}}{\sqrt{x}}\right),
\end{aligned}
\tag{42}
$$

respectively.

References

[1] E. Komatsu *et al.* [WMAP Collaboration], Astrophys. J. Suppl. **192**, 18 (2011).

[2] E. Aprile *et al.* [XENON100 Collaboration], Phys. Rev. Lett. **105**, 131302 (2010).

[3] E. Aprile *et al.* [XENON100 Collaboration], arXiv:1103.0303 [hep-ex].

[4] M. Drees, M. M. Nojiri, D. P. Roy and Y. Yamada, Phys. Rev. D **56**, 276 (1997) [Erratum-ibid. D **64**, 039901 (2001)]

[5] J. Hisano, S. Matsumoto, M. M. Nojiri and O. Saito, Phys. Rev. D **71**, 015007 (2005).

[6] M. Cirelli, N. Fornengo, A. Strumia, Nucl. Phys. B **753**, 178 (2006) .

[7] R. Essig, Phys. Rev. D **78**, 015004 (2008).

[8] J. Hisano, K. Ishiwata and N. Nagata, Phys. Lett. B **690**, 311 (2010).

[9] M. Cirelli, A. Strumia, and M. Tamburini, Nucl. Phys. B **787**, 152 (2007) .

[10] J. Hisano, S. Matsumoto, M. Nagai, O. Saito and M. Senami, Phys. Lett. B **646**, 34 (2007).

[11] J. Hisano, S. Matsumoto, M. Nojiri, Phys. Rev. Lett. **92**, 031303 (2004).

[12] J. Hisano, S. Matsumoto, M. M. Nojiri and O. Saito, Phys. Rev. D **71**, 063528 (2005).

[13] M. Drees and M. Nojiri, Phys. Rev. D **48**, 3483 (1993)

[14] J. Hisano, K. Ishiwata and N. Nagata, Phys. Rev. D **82**, 115007 (2010).

[15] G. Jungman, M. Kamionkowski and K. Griest, Phys. Rept. **267**, 195 (1996).

[16] H. D. Politzer, Nucl. Phys. B **172**, 349 (1980).

[17] A. Corsetti and P. Nath, Phys. Rev. D **64**, 125010 (2001).

[18] H. Ohki *et al.*, Phys. Rev. D **78**, 054502 (2008).

[19] H. Y. Cheng, Phys. Lett. B **219**, 347 (1989).

[20] J. Pumplin, D. R. Stump, J. Huston, H. L. Lai, P. M. Nadolsky and W. K. Tung, JHEP **0207**, 012 (2002).

[21] J. Hisano, K. Ishiwata, N. Nagata and M. Yamanaka, arXiv:1012.5455 [hep-ph].

[22] D. Adams *et al.* [Spin Muon Collaboration], Phys. Lett. B **357**, 248 (1995).

[23] A. Djouadi and M. Drees, Phys. Lett. B **484**, 183 (2000).